$B \to K_2^*(1430)\ell^+\ell^-$ distributions at large recoil in the Standard Model and beyond

Diganta Das,[1,*] Bharti Kindra,[2,3,†] Girish Kumar,[4,‡] and Namit Mahajan[2,§]

[1]*Department of Physics and Astrophysics, University of Delhi, Delhi 110007, India*
[2]*Physical Research Laboratory, Navrangpura, Ahmedabad 380 009, India*
[3]*Indian Institute of Technology Gandhinagar, Chandkheda, Ahmedabad 382 424, India*
[4]*Department of Theoretical Physics, Tata Institute of Fundamental Research, 1 Homi Bhabha Road, Mumbai 400005, India*

(Received 4 January 2019; published 30 May 2019)

We study the rare decay $B \to K_2^*(1430)(\to K\pi)\ell^+\ell^-$ in the Standard Model and beyond. Working in the transversity basis, we exploit the relations between the heavy-to-light form factors in the limit of heavy quark ($m_b \to \infty$) and large energy ($E_{K_2^*} \to \infty$) of the K_2^* meson. This allows us to construct observables where, at leading order in $\Lambda_{\rm QCD}/m_b$ and α_s, the form-factor dependence involving the $B \to K_2^*$ transitions cancels. Higher-order corrections are systematically incorporated in the numerical analysis. In the Standard Model, the decay has a sizable branching ratio, and therefore a large number of events can be expected at LHCb. Going beyond the Standard Model, we explore the implications of the global fit to presently available $b \to s\ell^+\ell^-$ data on the $B \to K_2^*\ell^+\ell^-$ observables.

DOI: 10.1103/PhysRevD.99.093012

I. INTRODUCTION

In the ongoing endeavor to unravel the flavor structure at the electroweak scale, the b-flavored mesons have played a very important role. In this effort, the exclusive B-meson decays that are induced by the $b \to s\ell^+\ell^-$ flavor-changing neutral current transition are sensitive to physics in and beyond the Standard Model (SM), also known as the new physics (NP). Well-known candidates of this type of decay, the $B \to (K, K^*)\ell^+\ell^-$, are at the center of theoretical and experimental investigations at present. Recent measurements of the observables $R_{K^{(*)}} \equiv \mathrm{BR}(B \to K^{(*)}\mu^+\mu^-)/\mathrm{BR}(B \to K^{(*)}e^+e^-)$ have shown hints of violation of lepton flavor universality (LFU). More explicitly, the LHCb Collaboration has measured $R_K^{\rm LHCb} = 0.745 \pm^{0.090}_{0.074} \pm 0.036$ in $q^2 \in [1, 6]\ \mathrm{GeV}^2$ [1], $R_{K^*}^{\rm LHCb} = 0.66^{+0.11}_{-0.07} \pm 0.03$ in $q^2 \in [0.045, 1.1]\ \mathrm{GeV}^2$, and $R_{K^*}^{\rm LHCb} = 0.69^{+0.11}_{-0.07} \pm 0.05$ in $q^2 \in [1.1, 6]\ \mathrm{GeV}^2$ [2] and finds departure from the SM prediction $R_{K^{(*)}} \sim 1$ by about $2-3\sigma$. Other notable deviations include the anomaly in the P_5' [3] observed in recent measurements 9–4]], and the systematic deficit in the $B_s \to \phi\mu^+\mu^-$ branching ratio [10]. Global fits to these $b \to s\ell^+\ell^-$ data [3,11–24] suggest that NP contributions to the Wilson coefficients can alleviate some of these tensions.

If the anomalies are indeed due to NP, they will show up in other $b \to s\ell^+\ell^-$ mediated transitions as well. The decay $B \to K_2^*(1430)\ell^+\ell^-$, where K_2^* is a tensor meson, is very similar to the well-studied $B \to K^*\ell^+\ell^-$ and can provide complementary information to NP. While the closely related radiative mode $B \to K_2^*\gamma$ has already been observed by the *BABAR* [25] and Belle [26] Collaborations, the LHCb has done some studies around the $K_2^*(1430)$ resonance [27]. The measured branching ratio for $B \to K_2^*\gamma$ is comparable to that with $B \to K^*\gamma$, which implies that the mode $B \to K_2^*\ell^+\ell^-$ also has a sizable branching ratio, which has been confirmed by direct computations [28–31].

The short-distance physics of $B \to K_2^*\ell^+\ell^-$ is contained in the perturbatively calculable Wilson coefficients. The long-distance physics of $B \to K_2^*$ hadronic matrix elements is parametrized in terms of the form factors, and the parametrization is similar to that of $B \to K^*$ hadronic matrix elements [31]. The form factors have

*diganta99@gmail.com
†bharti@prl.res.in
‡girishk@theory.tifr.res.in
§nmahajan@prl.res.in

been calculated [32] in a perturbative QCD approach using light-cone distribution amplitudes [33], and in light-cone sum rules in conjunction with the B-meson wave function [34]. Calculations in the light-cone QCD sum rule approach can be found in Ref. [35]. Using different form factors, phenomenological analysis of $B \to K_2^* \ell^+ \ell^-$ has been performed in many works [28,31,36–40]. The majority of these works have focused on simple observables like decay rate, forward-backward asymmetry of the dilepton system, and the polarization fractions of K_2^*. In Ref. [28], the fourfold angular distribution of decay products of K_2^* has been analyzed in the SM. In Ref. [38], the decay $B \to K_2^*(\to K\pi)\ell^+\ell^-$ was studied in the SM as well as in nonuniversal Z' and vectorlike quark models, but the branching fraction of the decay $K_2^* \to K\pi$ was ignored in their analysis. In this paper, building upon the previous works, we study the full fourfold angular distribution of $B \to K_2^*(\to K\pi)\ell^+\ell^-$ decay in the low dilepton invariant mass squared q^2 or large recoil of the K_2^* meson. In this region, the heavy quark ($m_b \to \infty$) and large recoil ($E_{K_2^*} \to \infty$) imply relations between $B \to K_2^*$ form factors. These relations reduce the number of independent form factors from seven to two. This helps us construct "clean" observables, where the form-factor dependence cancels at the leading order in $\Lambda_{\rm QCD}/m_b$ and α_s, making them suitable probes of NP. We have presented the determinations of the clean observables in the SM and studied the implications of global fits to the present $b \to s\ell^+\ell^-$ data.

The rest of the paper is organized as follows: In Sec. II, we discuss the general effective Hamiltonian and relevant operators for $b \to s\ell^+\ell^-$. In Sec. III, the hadronic matrix elements for $B \to K_2^*$ and their parametrization in terms of form factors are discussed. In Sec. IV, we discuss the $B \to K_2^*$ helicity amplitudes in the transversity basis and give their expressions in terms of form factors and short-distance Wilson coefficients. In Sec. V, we discuss $B \to K_2^*\ell^+\ell^-$ in the large recoil and large energy limit in detail. In Sec. VI, the four-body fully differential angular distribution and angular observables for $B \to K_2^*(\to K\pi)\ell^+\ell^-$ are discussed. In Sec. VII, we discuss the considered angular observables in the SM and in interesting NP scenarios. We give numerical predictions for observables and discuss their sensitivity to possible NP in $b \to s\ell^+\ell^-$. Finally, in Sec. VIII, we summarize the results of this paper.

II. EFFECTIVE HAMILTONIAN

We work with the following low-energy effective Hamiltonian for the rare $|\Delta B| = |\Delta S| = 1$ transition:

$$\mathcal{H}_{\rm eff} = -\frac{4G_F}{\sqrt{2}} V_{tb} V_{ts}^* \frac{\alpha_e}{4\pi} \times \sum_{i=7,9,10} [C_i(\mu)\mathcal{O}_i(\mu) + C_i'(\mu)\mathcal{O}_i'(\mu)], \quad (1)$$

where

$$\mathcal{O}_7^{(\prime)} = \frac{m_b}{e}[\bar{s}\sigma^{\mu\nu}P_R(P_L)b]F_{\mu\nu},$$
$$\mathcal{O}_9^{(\prime)} = [\bar{s}\gamma_\mu P_L(P_R)b][\bar{\ell}\gamma^\mu \ell],$$
$$\mathcal{O}_{10}^{(\prime)} = [\bar{s}\gamma_\mu P_L(P_R)b][\bar{\ell}\gamma^\mu\gamma_5 \ell]. \quad (2)$$

Here μ is the renormalization scale, α_e is the fine structure constant, $F_{\mu\nu}$ is the electromagnetic field strength tensor, and $P_{L/R} = (1 \mp \gamma_5)/2$ are the chiral projectors. The b-quark mass multiplying the dipole operator is assumed to be the running quark mass in the modified minimal-subtraction ($\overline{\rm MS}$) mass scheme. The contributions of the factorizable quark-loop corrections to current-current and penguin operators are absorbed in the effective Wilson coefficients $C_{7,9}^{\rm eff}$, as described in the Appendix A. All the SM Wilson coefficients are evaluated at the renormalization scale, $\mu = m_b = 4.2$ GeV [41]. For simplicity, we will neglect the superscript "eff" in the rest of the text. We ignore the nonfactorizable corrections to the Hamiltonian, which are expected to be significant at large recoil [42,43]. The primed Wilson coefficients are zero in the SM but can appear in some NP models. We will not consider NP contributions to $\mathcal{O}_7$, since these are well constrained [44].

III. $B \to K_2^*$ HADRONIC MATRIX ELEMENTS

We work in the B-meson rest frame and denote by p, k, p_{ℓ^+}, p_{ℓ^-} the four-momenta of the B-meson, the K_2^*, and the positively and negatively charged leptons, respectively. The tensor meson of the spin-2 polarization tensor $\epsilon^{\mu\nu}(n)$, where the helicities are $n = t$, 0, ±1, ±2, satisfies $\epsilon^{\mu\nu}k_\nu = 0$. In the final state, the K_2^* meson is partnered with two spin-1/2 leptons, and hence the K_2^* can only have helicities $n = t$, 0, ±1. Noting that the polarization tensor of the spin-2 state K_2^* can be conveniently written in terms of polarization vectors of a spin-1 state [45], we introduce a new polarization vector $\epsilon_{T\mu}$ (see Appendix B), in terms of which the $B \to K_2^*$ hadronic matrix elements can be written as [32]

$$
\begin{aligned}
\langle K_2^*(k,n)|\bar{s}\gamma^\mu b|\bar{B}(p)\rangle &= -\frac{2V(q^2)}{m_B+m_{K_2^*}}\epsilon^{\mu\nu\rho\sigma}\epsilon^*_{T\nu}p_\rho k_\sigma,\\
\langle K_2^*(k,n)|\bar{s}\gamma^\mu\gamma_5 b|\bar{B}(p)\rangle &= 2im_{K_2^*}A_0(q^2)\frac{\epsilon_T^*\cdot q}{q^2}q^\mu + i(m_B+m_{K_2^*})A_1(q^2)\left[\epsilon^*_{T\mu}-\frac{\epsilon_T^*\cdot q}{q^2}q^\mu\right]\\
&\quad - iA_2(q^2)\frac{\epsilon_T^*\cdot q}{m_B+m_{K_2^*}}\left[P^\mu-\frac{m_B^2-m_{K_2^*}^2}{q^2}q^\mu\right],\\
\langle K_2^*(k,n)|\bar{s}q_\nu\sigma^{\mu\nu}b|\bar{B}(p)\rangle &= -2iT_1(q^2)\epsilon^{\mu\nu\rho\sigma}\epsilon^*_{T\nu}p_{B\rho}p_{K\sigma},\\
\langle K_2^*(k,n)|\bar{s}q_\nu\sigma^{\mu\nu}\gamma_5 b|\bar{B}(p)\rangle &= T_2(q^2)[(m_B^2-m_{K_2^*}^2)\epsilon^*_{T\mu}-\epsilon_T^*\cdot qP^\mu]+T_3(q^2)\epsilon_T^*\cdot q\left[q^\mu-\frac{q^2(p+k)^\mu}{m_B^2-m_{K_2^*}^2}\right],
\end{aligned}
\tag{3}
$$

where $q = p_{\ell^+} + p_{\ell^-} = p - k$ is the momentum transfer.

IV. TRANSVERSITY AMPLITUDES

Corresponding to the effective Hamiltonian (1), the $B \to K_2^*\ell^+\ell^-$ amplitude for a given helicity of the K_2^* can be written as

$$
\begin{aligned}
\mathcal{A}(n) = -\frac{G_F}{\sqrt{2}}V_{tb}V_{ts}^*\frac{\alpha_e}{\pi}\Bigg(\Bigg[&(C_9-C_{10})\langle K_2^*(k,n)|\bar{s}\gamma^\mu P_L b|\bar{B}(p)\rangle - i\frac{2C_7m_b}{q^2}\langle K_2^*(k,n)|\bar{s}\sigma^{\mu\nu}q_\nu P_R b|\bar{B}(p)\rangle\\
&+(C_9'-C_{10}')\langle K_2^*(k,n)|\bar{s}\gamma^\mu P_R b|\bar{B}(p)\rangle\Bigg]\bar{\ell}\gamma_\mu P_L\ell + [C_{10}\to -C_{10}, C_{10}'\to -C_{10}']\bar{\ell}\gamma_\mu P_R\ell\Bigg).
\end{aligned}
\tag{4}
$$

The differential distribution for the decay can be calculated using helicity amplitudes $H_\pm^{L,R}$ and $H_0^{L,R}$, which are defined as the projections of the hadronic amplitudes on the polarization vectors of the gauge boson that creates a dilepton pair. Here the superscripts L, R correspond to the chiralities of the leptonic current. However, for comparison with the literature, we introduce the so-called transversity amplitudes, which are linear combinations of helicity amplitudes: $A_{\parallel L,R} = (H_+^{L,R} + H_-^{L,R})/\sqrt{2}$, $A_{\perp L,R} = (H_+^{L,R} - H_-^{L,R})/\sqrt{2}$, and $A_{0L,R} = H_0^{L,R}$. The expressions of the transversity amplitudes for $B \to K_2^*(\to K\pi)\ell^+\ell^-$ read [38]

$$
\begin{aligned}
A_{0L,R} = N\frac{\sqrt{\lambda}}{\sqrt{6}m_Bm_{K_2^*}}\frac{1}{2m_{K_2^*}\sqrt{q^2}}\Bigg[&(C_{9-}\mp C_{10-})\left[(m_B^2-m_{K_2^*}^2-q^2)(m_B+m_{K_2^*})A_1-\frac{\lambda}{m_B+m_{K_2^*}}A_2\right]\\
&+2m_bC_7\left[(m_B^2+3m_{K_2^*}^2-q^2)T_2-\frac{\lambda}{m_B^2-m_{K_2^*}^2}T_3\right]\Bigg],
\end{aligned}
\tag{5}
$$

$$
A_{\perp L,R} = -\sqrt{2}\frac{\sqrt{\lambda}}{\sqrt{8}m_Bm_{K_2^*}}N\left[(C_{9+}\mp C_{10+})\frac{\sqrt{\lambda}V}{m_B+m_{K_2^*}}+\frac{2m_bC_7}{q^2}\sqrt{\lambda}T_1\right],
\tag{6}
$$

$$
A_{\parallel L,R} = \sqrt{2}\frac{\sqrt{\lambda}}{\sqrt{8}m_Bm_{K_2^*}}N\left[(C_{9-}\mp C_{10-})(m_B+m_{K_2^*})A_1+\frac{2m_bC_7}{q^2}(m_B^2-m_{K_2^*}^2)T_2\right],
\tag{7}
$$

$$
A_t = 2\frac{\sqrt{\lambda}}{\sqrt{6}m_Bm_{K_2^*}}N[C_{10-}]A_0,
\tag{8}
$$

where the normalization constant is given by

$$N = \left[\frac{G_F^2\alpha_e^2}{3\cdot 2^{10}\pi^5 m_B^3}|V_{tb}V_{ts}^*|^2\lambda^{1/2}(m_B^2, m_{K_2^*}^2, q^2) \times \mathcal{B}(K_2^* \to K\pi)\beta_\ell\right]^{\frac{1}{2}},$$
$$\beta_\ell = \sqrt{1-\frac{4m_\ell^2}{q^2}}. \tag{9}$$

Here $\lambda(a,b,c) = a^2+b^2+c^2-2(ab+bc+ca)$, and we have defined

$$C_{9\pm} = C_9 \pm C_9', \qquad C_{10\pm} = C_{10} \pm C_{10}'. \tag{10}$$

V. HEAVY-TO-LIGHT FORM FACTORS AT LARGE RECOIL

The $B \to K_2^*$ hadronic matrix elements, parametrized in terms of form factors in Eq. (3), are nonperturbative in nature and constitute the dominant uncertainty in theoretical predictions. In the absence of any lattice calculations of the form factors at present, the uncertainty can be reduced by making use of the relations between the form factors that originate in the limit of heavy quark $m_b \to \infty$ of the initial meson and large energy $E_{K_2^*}$ of the final meson [46,47]. In these limits, the heavy-to-light form factors can be expanded in small ratios of $\Lambda_{\rm QCD}/m_b$ and $\Lambda_{\rm QCD}/E_{K_2^*}$. To leading order in $\Lambda_{\rm QCD}/m_b$ and α_s, the large-energy symmetry dictates that there are only two independent universal soft form factors, $\xi_\parallel(q^2)$ and $\xi_\perp(q^2)$ [47], in terms of which the rest of the form factors can be written as [31]

$$A_0(q^2) = \frac{m_{K_2^*}}{|p_{K_2^*}|}\left[\left(1-\frac{m_{K_2^*}^2}{m_B}\right)\xi_\parallel(q^2) + \frac{m_{K_2^*}}{m_B}\xi_\perp(q^2)\right],$$
$$A_1(q^2) = \frac{m_{K_2^*}}{|p_{K_2^*}|}\frac{2E_{K_2^*}}{m_B+m_{K_2^*}}\xi_\perp(q^2), \qquad A_2(q^2) = \frac{m_{K_2^*}}{|p_{K_2^*}|}\left(1+\frac{m_{K_2^*}}{m_B}\right)\left[\xi_\perp(q^2) - \frac{m_{K_2^*}}{E}\xi_\parallel\right],$$
$$V(q^2) = \frac{m_{K_2^*}}{|p_{K_2^*}|}\left(1+\frac{m_{K_2^*}}{m_B}\right)\xi_\perp, \qquad T_1(q^2) = \frac{m_{K_2^*}}{|p_{K_2^*}|}\xi_\perp(q^2),$$
$$T_2(q^2) = \frac{m_{K_2^*}}{|p_{K_2^*}|}\left(1-\frac{q^2}{m_B^2-m_{K_2^*}^2}\right)\xi_\perp(q^2), \qquad T_3(q^2) = \frac{m_{K_2^*}}{|p_{K_2^*}|}\left[\xi_\perp - \left(1-\frac{m_{K_2^*}^2}{m_B^2}\right)\frac{m_{K_2^*}}{E}\xi_\parallel(q^2)\right]. \tag{11}$$

Here recoil energy $E_{K_2^*}$ is given by

$$E_{K_2^*} = \frac{m_B}{2}\left(1-\frac{q^2}{m_B^2}+\frac{m_{K_2^*}^2}{m_B^2}\right). \tag{12}$$

The q^2 dependence of the soft form factors $\xi_\perp(q^2)$ and $\xi_\parallel(q^2)$ is given by [31,47]

$$\xi_{\parallel,\perp}(q^2) = \frac{\xi_{\parallel,\perp}(0)}{(1-q^2/m_B^2)^2}. \tag{13}$$

The values of the soft form factors at zero recoil $q^2=0$ have been estimated using the Bauer-Stech-Wirbel (BSW) model [48] in Ref. [31]. In Ref. [30], these are also extracted from experimental data on $B \to K^*\gamma$ from *BABAR* [25] and Belle [26]. For our numerical analysis we have used the values $\xi_\perp(0) = 0.29 \pm 0.09$ and $\xi_\parallel(0) = 0.26 \pm 0.10$, which were obtained in Ref. [32] in a perturbative QCD approach utilizing the nontrivial relations realized in the large-energy limit. These estimates are consistent with the ones obtained in Refs. [30,31] but have large errors. Not to be too conservative in our theory estimates, we choose to use the values given above.

Substituting Eq. (11) into Eq. (5), we obtain at leading order in $\Lambda_{\rm QCD}/m_b$ and α_s the simple expressions of the transversity amplitudes in terms of soft form factors $\xi_\parallel$ and $\xi_\perp$ as

$$A_{0L(R)} = \sqrt{\frac{2}{3}}\frac{N}{\sqrt{q^2}}m_B^2\left(1-\frac{q^2}{m_B^2}\right) \times \left((C_{9-} \mp C_{10+}) + 2C_7\frac{m_b}{m_B}\right)\xi_\parallel(q^2), \tag{14}$$

$$A_{\perp L(R)} = -Nm_B\left(1-\frac{q^2}{m_B^2}\right) \times \left((C_{9+} \mp C_{10+}) + 2C_7\frac{m_b m_B}{q^2}\right)\xi_\perp(q^2), \tag{15}$$

$$A_{\parallel L(R)} = N m_B \left(1 - \frac{q^2}{m_B^2}\right) \times \left((C_{9-} \mp C_{10-}) + 2C_7 \frac{m_b m_B}{q^2}\right) \xi_\perp(q^2), \quad (16)$$

$$A_t = 2\frac{\sqrt{\lambda}}{\sqrt{6} m_B m_{K_2^*}} N \frac{2 m_{K_2^*} m_B}{\sqrt{\lambda}} \times \left(\left(1 - \frac{m_{K_2^*}^2}{m_B E_{K_2^*}}\right)\xi_\parallel + \frac{m_{K_2^*}}{m_B}\xi_\perp\right) C_{10-}. \quad (17)$$

At this point, we recall that the relations (11) are derived in the QCD factorization (QCDf) and soft collinear effective theory (SCET) approach in which the factorization formula for the heavy-to-light $B \to K_2^*$ form factors are

$$F_i(q^2) = (1 + \mathcal{O}(\alpha_s))\xi + \Phi_B \oplus T_i \oplus \Phi_{K_2^*} + \mathcal{O}(\Lambda_{\rm QCD}/m_b). \quad (18)$$

Here T_i are the perturbatively calculable hard scattering kernels, and Φ_{B,K^*} are the hadron distribution amplitudes, which are nonperturbative objects. There are no means to calculate the $\Lambda_{\rm QCD}/m_b$ corrections at present, and therefore the cancellations of soft form factors in the clean observables are valid only at leading order in $\Lambda_{\rm QCD}/m_b$. The neglected higher-order terms add to the uncertainty of our theoretical predictions. We use the ensemble method following Ref. [49] to account for $\Lambda_{\rm QCD}/m_b$ uncertainties in our numerical analysis of observables. This is done by multiplying the transversity amplitudes by correction factors:

$$A_{0,\parallel,\perp} \to A_{0,\parallel,\perp}(1 + c_{0,\parallel,\perp}), \quad (19)$$

where $c_{0,\parallel,\perp}$ are the correction factors defined as $c_{0,\parallel,\perp} = |c_{0,\parallel,\perp}|e^{i\theta_{0,\parallel,\perp}}$. We vary $|c_{0,\parallel,\perp}|$ and $\theta_{0,\parallel,\perp}$ in a random uniform distribution in the ranges $[-0.1, 0.1]$ and $[-\pi, \pi]$, respectively. Other sources of uncertainty are due to the variation of scale μ between $m_b/2$ and $2m_b$, and the ratio m_c/m_b. Some of the inputs and their uncertainties are listed in Table I.

TABLE I. The numerical inputs used in our analysis. The values of α_s, α_e, and $m_b^{\overline{\rm MS}}$ at low scale $\mu = 2.1$ GeV and high scale $\mu = 8.4$ GeV are also used from Ref. [41].

Parameter	Value	Source
m_B	5.279 GeV	[52]
$m_{K_2^*}$	1432.4 ± 1.3 MeV	[52]
$m_b^{\overline{\rm MS}}$	4.20 GeV	[41]
$m_b^{\rm pole}$	4.7417 GeV	[41]
$m_c^{\rm pole}$	1.5953 GeV	[41]
$\lvert V_{ts}^* V_{tb}\rvert$	0.04088 ± 0.00055	[53]
$\alpha_s(\mu = 4.2\ {\rm GeV})$	0.2233	[41]
$\alpha_e(\mu = 4.2\ {\rm GeV})$	1/133.28	[41]
${\rm Br}(K_2^* \to K\pi)$	$(49.9 \pm 1.2)\%$	[52]

VI. ANGULAR DISTRIBUTIONS AND OBSERVABLES

We assume that the K_2^* is on the mass shell, so that the $B \to K_2^*(\to K\pi)\ell^+\ell^-$ decay can be completely described in terms of only four kinematical variables: the lepton invariant mass squared q^2 and three angles θ_ℓ, θ_K, and ϕ. The lepton angle θ_ℓ is defined as the angle made by the negatively charged lepton ℓ^- with respect to the direction of the motion of the B meson in the dilepton rest frame. The angle θ_K is defined as the angle made by the K^- with respect to the opposite of the direction of the B meson in the $K\pi$ rest frame. The angle between the decay planes of the two leptons and the $K\pi$ is defined as ϕ. In terms of these variables, the fourfold differential distributions read [38]

$$\begin{aligned}\frac{d^4\Gamma}{dq^2 d\cos\theta_\ell d\cos\theta_K d\phi} = \frac{15}{128\pi}[&I_1^s 3\sin^2 2\theta_K + I_1^c(3\cos^2\theta_K - 1)^2 + I_2^s 3\sin^2 2\theta_K \cos 2\theta_l + I_2^c(3\cos^2\theta_K - 1)^2 \cos 2\theta_l \\ &+ I_3 3\sin^2 2\theta_K \sin^2\theta_l \cos 2\phi + I_4 2\sqrt{3}(3\cos^2\theta_K - 1)\sin 2\theta_K \sin 2\theta_l \cos\phi \\ &+ I_5 2\sqrt{3}(3\cos^2\theta_K - 1)\sin 2\theta_K \sin\theta_l \cos\phi + I_6 3\sin^2 2\theta_K \cos\theta_l \\ &+ I_7 2\sqrt{3}(3\cos^2\theta_K - 1)\sin 2\theta_K \sin\theta_l \sin\phi \\ &+ I_8 2\sqrt{3}(3\cos^2\theta_K - 1)\sin 2\theta_K \sin 2\theta_l \sin\phi \\ &+ I_9 3\sin^2 2\theta_K \sin^2\theta_l \sin 2\phi]. \end{aligned} \quad (20)$$

The distribution bears some resemblance to the $B \to K^*\ell^+\ell^-$ angular distribution [50,51], which is related to the fact that $B \to K_2^*\ell^+\ell^-$ decay involves a K_2^* meson with polarization $t, 0, \pm 1$ only, as discussed in Appendix B.

The differences can be attributed to the different spherical harmonics required to describe the strong decays of K^* and K_2^*. The angular coefficients $I_i(q^2)$ can be written in terms of the transversity amplitudes and are given in Appendix C. The decay rate for the CP-conjugate process is obtained by the replacements $I_{1,2,3,4,7} \to \bar{I}_{1,2,3,4,7}$ and $I_{5,6,8,9} \to -\bar{I}_{5,6,8,9}$, where $\bar{I}$ is equal to I with all of the weak phase conjugated. In this paper, we will consider only CP-averaged observables, so that I means $I + \bar{I}$ and total decay width Γ stands for $\Gamma + \bar{\Gamma}$. At leading order $\Lambda_{\rm QCD}/m_b$ and α_s, the short- and long-distance physics factorize as

$$
\begin{aligned}
I_1^c &= \frac{2}{3}\frac{N^2}{q^2} m_B^4 \left(1-\frac{q^2}{m_B^2}\right)^2 \left[|\sigma_-|^2 + |\sigma_+|^2 + \frac{8m_\ell^2}{q^2}\left\{\mathrm{Re}(\sigma_-\sigma_+^*) + 2|C_{10-}|^2\left(1 - \frac{2m_{K_2^*}^2}{m_B^2 - q^2} + \frac{m_{K_2^*}}{m_B}\frac{\xi_\perp}{\xi_\parallel}\right)^2\right\}\right]\xi_\parallel^2,\\
I_1^s &= \frac{3}{4} N^2 m_B^2 \left(1-\frac{q^2}{m_B^2}\right)^2 \left[\left(1-\frac{4m_\ell^2}{3q^2}\right)\{(|\rho_-^L|^2 + |\rho_+^L|^2) + (L \leftrightarrow R)\} + \frac{m_\ell^2}{3q^2}\mathrm{Re}(\rho_-^L\rho_-^{R*} + \rho_+^L\rho_+^{R*})\right]\xi_\perp^2,\\
I_2^c &= -\frac{2}{3}\frac{N^2}{q^2} m_B^4 \beta_\ell^2 \left(1-\frac{q^2}{m_B^2}\right)^2 (|\sigma_-|^2 + |\sigma_+|^2)\xi_\parallel^2,\\
I_2^s &= \frac{1}{4} N^2 m_B^2 \beta_\ell^2 \left(1-\frac{q^2}{m_B^2}\right)^2 \{(|\rho_-^L|^2 + |\rho_+^L|^2) + (L \leftrightarrow R)\}\xi_\perp^2,\\
I_3 &= \frac{1}{2} N^2 m_B^2 \beta_\ell^2 \left(1-\frac{q^2}{m_B^2}\right)^2 \{(|\rho_+^L|^2 - |\rho_-^L|^2) + (L \leftrightarrow R)\}\xi_\perp^2,\\
I_4 &= \frac{1}{\sqrt{3}}\frac{N^2}{\sqrt{q^2}} m_B^3 \beta_\ell^2 \left(1-\frac{q^2}{m_B^2}\right)^2 \mathrm{Re}[\sigma_-\rho_-^{L*} + \sigma_+\rho_-^{R*}]\xi_\perp\xi_\parallel,\\
I_5 &= -\frac{2}{\sqrt{3}}\frac{N^2}{\sqrt{q^2}} m_B^3 \beta_\ell \left(1-\frac{q^2}{m_B^2}\right)^2 \mathrm{Re}[\sigma_-\rho_+^{L*} - \sigma_+\rho_+^{R*}]\xi_\perp\xi_\parallel,\\
I_6 &= -2N^2 m_B^2 \beta_\ell \left(1-\frac{q^2}{m_B^2}\right)^2 \mathrm{Re}[(\rho_-^L\rho_+^{L*}) - (L \leftrightarrow R)]\xi_\perp^2,\\
I_7 &= \frac{2}{\sqrt{3}}\frac{N^2}{\sqrt{q^2}} m_B^3 \beta_\ell \left(1-\frac{q^2}{m_B^2}\right)^2 \mathrm{Im}[\sigma_-\rho_-^{L*} - \sigma_+\rho_-^{R*}]\xi_\perp\xi_\parallel,\\
I_8 &= -\frac{1}{\sqrt{3}}\frac{N^2}{\sqrt{q^2}} m_B^3 \beta_\ell^2 \left(1-\frac{q^2}{m_B^2}\right)^2 \mathrm{Im}[\sigma_-\rho_+^{L*} + \sigma_+\rho_+^{R*}]\xi_\perp\xi_\parallel,\\
I_9 &= -N^2 m_B^2 \beta_\ell^2 \left(1-\frac{q^2}{m_B^2}\right)^2 \mathrm{Im}[(\rho_-^L\rho_+^{L*}) + (L \leftrightarrow R)]\xi_\perp^2.
\end{aligned}
\tag{21}
$$

Here we have introduced the following combinations of short-distance Wilson coefficients:

$$\rho_\mp^L(q^2) = C_{9\mp} - C_{10\mp} + \frac{2m_b m_B}{q^2} C_7, \tag{22}$$

$$\rho_\mp^R(q^2) = C_{9\mp} + C_{10\mp} + \frac{2m_b m_B}{q^2} C_7, \tag{23}$$

$$\sigma_\mp(q^2) = C_{9-} \mp C_{10+} + \frac{2m_b}{m_B} C_7. \tag{24}$$

While writing Eq. (21), we have not displayed the explicit q^2 dependence of form factors $\xi_{\perp,\parallel}(q^2)$ and the Wilson coefficients $\rho_\mp^{L,R}(q^2)$ for simplicity. Note that in the SM basis, one has $\rho_-^L = \rho_+^L$ and $\rho_-^R = \rho_+^R$.

From the angular distribution (20), one can construct observables like the forward-backward asymmetry $A_{\rm FB}$, the longitudinal polarization fraction F_L, and the differential decay width $d\Gamma/dq^2$ as functions of dilepton invariant mass q^2. This can be done by weighted angular integrals of the fourfold differential distribution given in Eq. (20) as the following:

$$\mathcal{O}_i(q^2) = \int d\cos\theta_\ell\, d\cos\theta_K\, d\phi\, \mathcal{W}_i(\theta_\ell, \theta_K, \phi) \times \frac{d^4\Gamma}{dq^2 d\cos\theta_\ell d\cos\theta_K d\phi}, \tag{25}$$

from which various angular observables can be extracted by the suitable choices for weight function $\mathcal{W}_i(\theta_\ell, \theta_K, \phi)$:

TABLE II. Binned predictions for $\mathrm{BR}(B \to K_2^*\mu^+\mu^-)$, F_L, and A_{FB} in the SM. Theoretical errors correspond to uncertainties in the form factors, $\Lambda_{\mathrm{QCD}}/m_b$ correction effects, and errors in inputs, as discussed in the text.

Observable / q^2 bin (GeV^2)	[0.1–1.0]	[1.0–2.0]	[2.0–4.0]	[4.0–6.0]	[1.0–6.0]
$10^7 \times \langle \mathrm{BR}(B \to K_2^*\mu\mu) \rangle$	0.204 ± 0.093	0.104 ± 0.056	0.197 ± 0.113	0.233 ± 0.124	0.534 ± 0.292
$\langle F_L \rangle$	0.350 ± 0.199	0.691 ± 0.205	0.764 ± 0.188	0.684 ± 0.207	0.714 ± 0.201
$\langle A_{\mathrm{FB}} \rangle$	0.092 ± 0.028	0.193 ± 0.127	0.066 ± 0.056	-0.135 ± 0.089	0.001 ± 0.018

(1) The full differential decay width $d\Gamma/dq^2$ is simply obtained by choosing $\mathcal{W}_\Gamma = 1$,

$$\frac{d\Gamma}{dq^2} = \frac{1}{4}(3I_1^c + 6I_1^s - I_2^c - 2I_2^s). \tag{26}$$

(2) The forward-backward asymmetry of lepton pair A_{FB} (normalized by differential decay width) is extracted with $\mathcal{W}_{A_{\mathrm{FB}}} = \mathrm{sgn}[\cos\theta_\ell]/(d\Gamma/dq^2)$,

$$A_{\mathrm{FB}}(q^2) = \frac{3I_6}{3I_1^c + 6I_1^s - I_2^c - 2I_2^s}. \tag{27}$$

(3) The longitudinal polarization fraction F_L (normalized by differential decay width) is extracted with $\mathcal{W}_{F_L} = (3/2)(-3 + 7\cos^2\theta_K)/(d\Gamma/dq^2)$,

$$F_L(q^2) = \frac{3I_1^c - I_2^c}{3I_1^c + 6I_1^s - I_2^c - 2I_2^s}. \tag{28}$$

By definition, then, the transverse polarization fraction is $F_T = 1 - F_L$.

In Table II, we present our q^2-bin-averaged estimates for the above observables for $B \to K_2^*\mu^+\mu^-$ in different bins in the SM. The sources of uncertainties are $\Lambda_{\mathrm{QCD}}/m_b$ corrections, variation of the renormalization scale μ, form factors, and other numerical inputs. In Fig. 1, we have shown the dependence of these three observables on dilepton invariant mass q^2. As can be seen from this analysis, the $B \to K_2^*\mu^+\mu^-$

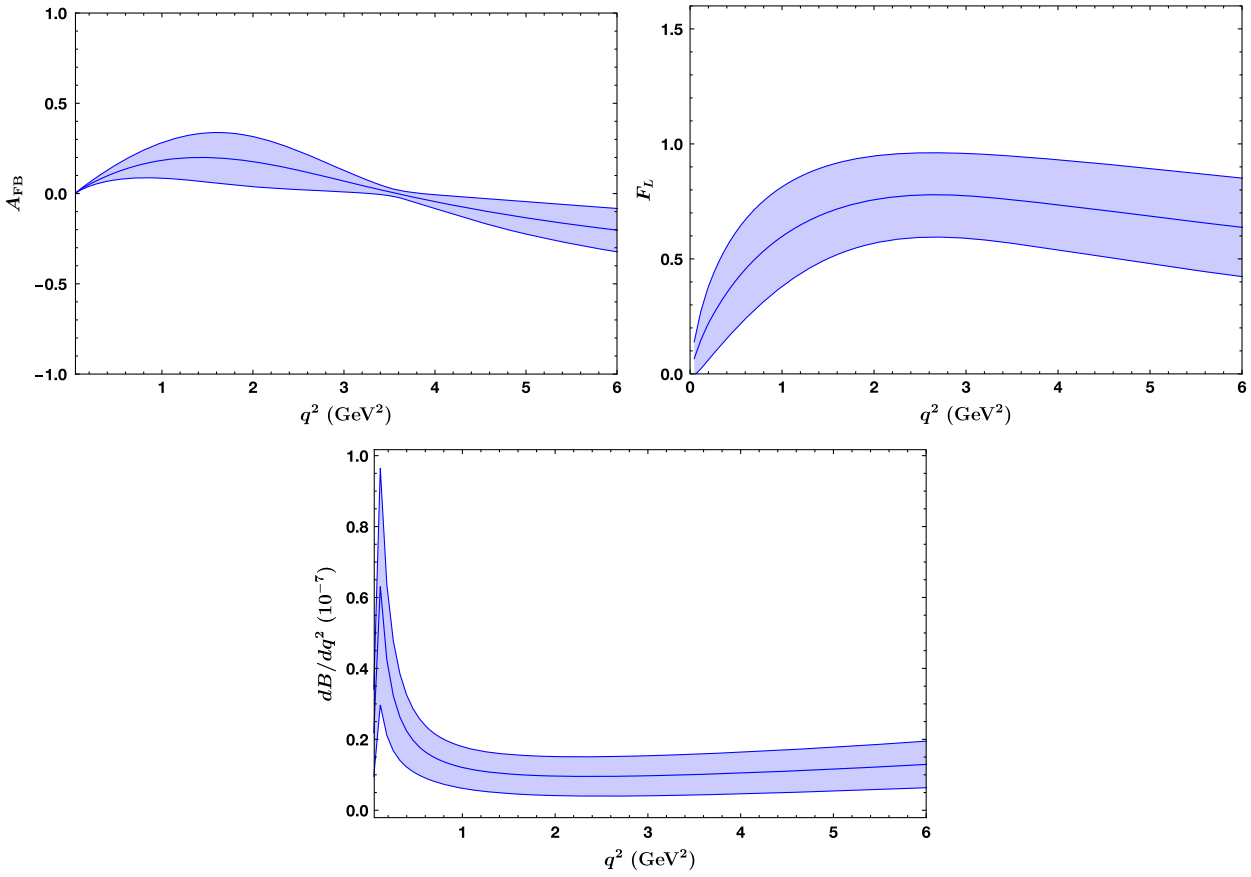

FIG. 1. Differential branching fraction $d\mathcal{B}/dq^2$, forward-backward asymmetry of the lepton pair, A_{FB}, and longitudinal polarization fraction, F_L, as functions of dimuon invariant mass q^2 for $B \to K_2^*\mu^+\mu^-$ in the SM. The bands show estimates of uncertainties due to errors in form factors and various inputs (discussed in the text) used for the evaluation of observables.

branching ratio is only 1 order of magnitude smaller than $B \to K^* \mu^+ \mu^-$. Therefore, $B \to K_2^* \mu^+ \mu^-$ can be a viable signal at future LHCb. However, due to their large-uncertainty branching ratios, $A_{\rm FB}$ and F_L are not suitable for searches of new physics.

The study of the fourfold angular distribution gives access to numerous observables that can be measured by the LHCb. Due to factorization of long- and short-distance physics at large recoil [Eq. (21)], one can construct observables in terms of ratios where the form factors cancel, making them highly sensitive to NP. In the context of decay $B \to K^*(\to K\pi)\mu^+\mu^-$, such observables have been constructed (see, e.g., Ref. [54] and references therein). Taking a cue from $B \to K^* \ell^+ \ell^-$ [54–56], we consider the following set of observables, where the soft form factor cancels at leading order in α_s and $\Lambda_{\rm QCD}/m_b$, making them a suitable probe for new physics:

$$\langle P_1 \rangle = \frac{1}{2}\frac{\int_{\rm bin} dq^2 I_3}{\int_{\rm bin} dq^2 I_2^s}, \quad \langle P_4 \rangle = \frac{\int_{\rm bin} dq^2 I_4}{\sqrt{-\int_{\rm bin} dq^2 I_2^c \int_{\rm bin} dq^2 I_2^s}}, \tag{29}$$

$$\langle P_2 \rangle = \frac{1}{8}\frac{\int_{\rm bin} dq^2 I_6}{\int_{\rm bin} dq^2 I_2^s}, \quad \langle P_5 \rangle = \frac{\int_{\rm bin} dq^2 I_5}{2\sqrt{-\int_{\rm bin} dq^2 I_2^c \int_{\rm bin} dq^2 I_2^s}}, \tag{30}$$

$$\langle P_3 \rangle = -\frac{1}{4}\frac{\int_{\rm bin} dq^2 I_9}{\int_{\rm bin} dq^2 I_2^s}, \quad \langle P_6 \rangle = \frac{\int_{\rm bin} dq^2 I_7}{2\sqrt{-\int_{\rm bin} dq^2 I_2^c \int_{\rm bin} dq^2 I_2^s}}. \tag{31}$$

The subleading corrections to them will be estimated following the discussions in Sec. V.

As also discussed in Sec. I, recent LHCb results [1,2] of measurements of the ratio of $B \to K(K^*)\ell^+\ell^-$ branching ratios of dimuons over dielectrons known as R_{K,K^*} show significant deviation from their SM predictions $R_{K,K^*} \sim 1$ [57], which hints at the violation of lepton-flavor universality. Observation of the same pattern of deviation in the K and K^* mode is quite intriguing and has attracted a lot of attention recently (see Ref. [58] for a model-independent analysis). If NP is to blame for these, such deviations should be seen in $B \to K_2^* \ell^+ \ell^-$ as well, and need to be studied. We define a similar ratio for $B \to K_2^* \ell^+ \ell^-$:

$$R_{K_2^*} = \frac{\mathcal{B}(B \to K_2^* \mu\mu)}{\mathcal{B}(B \to K_2^* ee)}. \tag{32}$$

Having discussed all the observables, we are now ready to proceed with the numerical analysis of these observables in the SM and NP scenarios in the next section.

VII. NUMERICAL ANALYSIS

In light of the recent flavor anomalies, several groups have performed global fits of Wilson coefficients to $b \to s\ell^+\ell^-$ data to decipher the pattern of NP [3,11–24]. These fits indicate that a negative contribution to the Wilson coefficient C_9^μ can alleviate the tension between theory and experimental data. There are other scenarios, as well, which lead to similar fits. Following Ref. [24], we consider three of them (called S1, S2, and S3) having the largest pull[1]:

S1. NP in C_9 only with $C_9^{\mu,\rm NP} = -1.02$, for which the pull is 5.8σ.

S2. In this scenario, NP is considered in both C_9 and C_{10}, but they are correlated, $C_9^{\mu,\rm NP} = -C_{10}^{\mu,\rm NP} = -0.49$, and the pull for this scenario is 5.4σ.

S3. In this scenario, NP is considered in C_9 and C_9' and again correlated with the best fit given by $C_9^{\mu,\rm NP} = -C_9'^{\mu,\rm NP} = -1.02$, for which the pull is 5.7σ.

Our main numerical results in the SM and the above three NP cases for all the angular observables considered in this work are collected in Appendix D. The binned predictions for clean observables are displayed in Fig. 2. To make binned average predictions of different observables, we simultaneously vary the form factors, $\Lambda_{\rm QCD}/m_b$ corrections, and other inputs within their allowed intervals. The resultant uncertainty on the observables corresponds to the union of uncertainties from all sources. In the case of observables where ratios are involved, we perform the integration in the numerator and denominator separately before taking the ratio. We restrict our analysis to the low dilepton invariant mass region and consider q^2 bins lying within the range 0.1–6.0 GeV^2. This region is sufficiently below the radiative tail of the charmonium resonances $J/\psi, \psi'$. Therefore, in our numerical analysis, apart from the perturbative $c\bar{c}$ contributions to the Wilson coefficients, the contributions from the charmonium resonances are not taken into account.

The branching fraction for $B \to K_2^* \mu^+ \mu^-$ in the SM is $\sim\mathcal{O}(10^{-7})$ (see Table II). In all three NP scenarios, we find consistently smaller central values for the branching fraction compared to the SM value. This is pertaining to the fact that the global analysis of $b \to s\ell^+\ell^-$ suggests a destructive NP contribution to C_9^μ. For $A_{\rm FB}$ (F_L), we find a slightly larger (smaller) central value in NP cases compared to the central SM value. However, as these observables ($d\Gamma/dq^2$, F_L, and $A_{\rm FB}$) are at present plagued by large theoretical errors, no striking deviation from the SM value is found. On the other hand, prospects for testing the NP hypothesis in $b \to s\ell^+\ell^-$ in some clean observables $P_i(q^2)$ are promising.

The clean observable P_1 depends on the angular coefficients I_3 and I_2, and is of special interest due to its remarkable sensitivity to right-handed currents. The $(V-A)$ structure of the SM renders the $H_\pm$ helicities of the $B \to K_2^* \ell^+ \ell^-$ suppressed, implying $|A_\parallel| \simeq |A_\perp|$. Therefore, this observable is predicted to be zero in the SM. A similar characteristic is also shared by its $B \to K^*$ counterpart, as

[1]pull $= \sqrt{\Delta\chi^2}$.

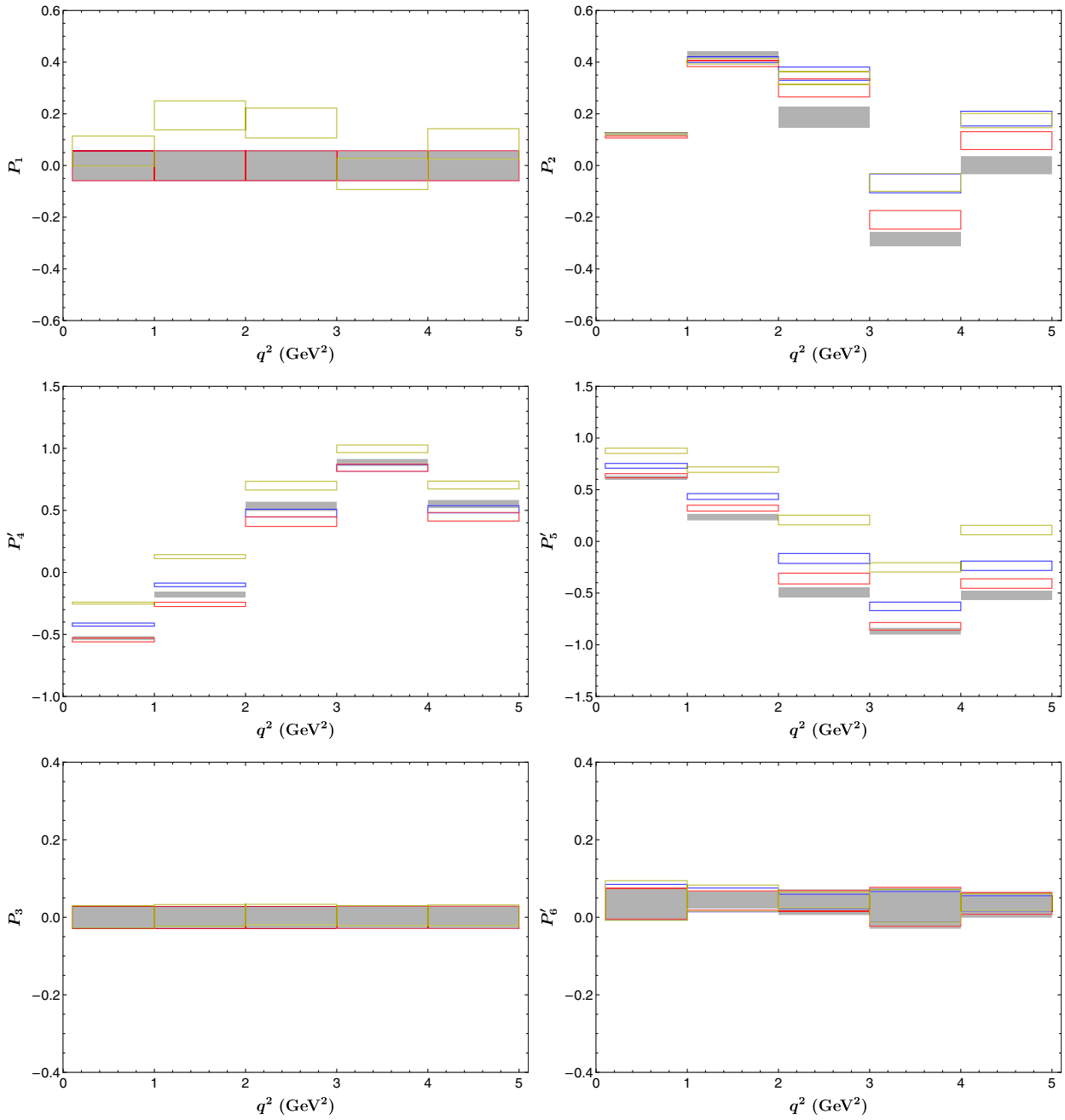

FIG. 2. The clean observables $P_i^{(\prime)}(q^2)$ $(i = 1, 2, 3, 4, 5, 6)$ in different q^2 bins in the SM (gray) and three NP scenarios S1 (blue), S2 (red), and S3 (yellow). The horizontal width of each box corresponds to the q^2 bin size, and the vertical length gives an estimate of uncertainties for that particular q^2 bin, as discussed in the text.

noted in Ref. [11]. As shown in Fig. 2, P_1 is consistent with zero in the SM and in the two scenarios S1 and S2 (which assume NP in the left-handed currents only), while a large deviation from $P_1 \simeq 0$ is found in scenario S3 (which has a nonzero value of the right-handed Wilson coefficient C_9'). The uncertainty bands correspond to various theory uncertainties. Since form factors cancel in ratio, the uncertainty is largely dominated by $\Lambda_{\rm QCD}/m_b$ corrections to the amplitudes which are modeled by Eq. (19). The observable P_2 is similar to forward-backward asymmetry $A_{\rm FB}$, but it is theoretically much cleaner. We note that its uncertainty is largely dominated by parametric errors including the scale μ. Similar to $A_{\rm FB}$, P_2 has larger values in all three NP scenarios. The zero crossing of P_2 (same as that of $A_{\rm FB}$)[2] lies within the $[2, 4]$ GeV^2 bin, and at the leading order is given by

[2]Note that since the numerators of P_2 and $A_{\rm FB}$ are the same, the zeros of both observables are also the same.

$$q_0^2(P_2) \simeq -\frac{2C_7}{C_9 - (C'_{10}/C_{10})C'_9} m_b m_B. \quad (33)$$

In order to obtain the above relation, we have used transversity amplitudes given in Eqs. (14)–(17) and assumed the Wilson coefficients to be real. This expression is identical to the corresponding observable for the $B \to K^*$ case. Note that the zero crossing $q_0^2(P_2)$ depends on the short-distance Wilson coefficients $C_9^{\ell(\prime)}$ and $C_{10}^{\ell(\prime)}$, and it has no dependence on the mass of the lepton in the final state. Consequently, in the SM it has the same value for all three decay modes, $B \to K_2^* \ell^+ \ell^-$ ($\ell = e, \mu, \tau$). Therefore, the zero crossing $q_0^2(P_2)$ turns out to be a good observable to test the hypothesis of lepton-flavor-universality-violating (LFUV) NP.

For observables P'_4 and P'_5, the largest deviations from the SM value are observed in scenario S3, thereby showing good sensitivity to right-handed NP. On the other hand, observables P_3 and P'_6 depend on $I_9(q^2)$ and $I_7(q^2)$, respectively. These two observables depend on the imaginary part of $\rho_\mp^{L,R}(q^2)$ and $\sigma_\mp(q^2)$. The imaginary part of the SM Wilson coefficient $C_{9,7}^{\rm eff}$ is very tiny, and therefore the SM predictions for P_3 and P'_6 are highly suppressed. Since in our numerical analysis we consider real NP Wilson coefficients, these observables remain suppressed in all three NP scenarios. Deviations in these observables, if seen in experiments, will be a sign of CP-violating NP, while for P_3, the dominant uncertainty is $\Lambda_{\rm QCD}/m_b$, and the errors in $P'_{4,5,6}$ are dominated by $\Lambda_{\rm QCD}/m_b$ corrections and parametric uncertainties.

Finally, in Fig. 3 we present our determinations of the LFUV ratio $R_{K_2^*}$. Similar observables for $B \to K^{(*)} \ell^+ \ell^-$ in the SM are predicted to be ~ 1 [57]. These LFUV ratios are exceptionally clean observables, with theoretical errors being at the level of only $\sim 1\%$, making them an ideal candidate to probe NP. As mentioned earlier, R_K and R_{K^*} have been measured experimentally, and both measurements are lower than the SM value, which could be interpreted as a sign of NP. Therefore, the measurement of $R_{K_2^*}$ can be important to corroborate the deviations seen in R_K and R_K^*. In all three NP scenarios, $R_{K_2^*}$ is suppressed compared to the SM value. For NP case S2, the deviations from unity are largest, while for NP case S3, the suppression is relatively smaller, as this solution contains a mixture of left-handed and right-handed currents, and right-handed currents tend to increase the value of ratio. The bin-averaged predictions for $R_{K_2}^*$ in the SM and NP cases are given in Appendix D.

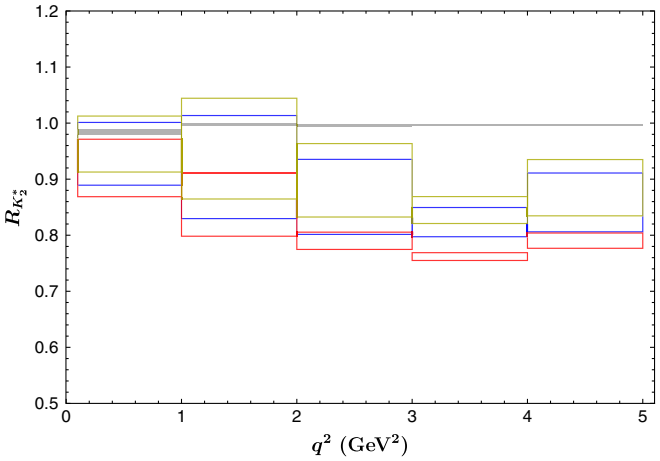

FIG. 3. Binned predictions for $R_{K_2^*}$ in the SM (gray) and NP scenarios S1 (blue), S2 (red), and S3 (yellow).

VIII. SUMMARY AND DISCUSSION

In this paper, we have performed an angular analysis of the exclusive semileptonic decay $B \to K_2^*(\to K\pi)\mu^+\mu^-$. The decay, at the quark level, is governed by the $b \to s\ell^+\ell^-$ FCNC transition. About $2-3\sigma$ discrepancies in $b \to s\ell^+\ell^-$ transitions have recently been observed in $B \to K(K^*)\ell^+\ell^-$ decays. If these discrepancies are due to NP, then similar anomalies are also expected in $B \to K_2^*(\to K\pi)\mu^+\mu^-$ transitions as well, which makes this decay worth studying.

A full angular distribution of $B \to K_2^*(\to K\pi)\mu^+\mu^-$ in the transversity basis, similar to $B \to K^*(\to K\pi)\mu^+\mu^-$, offers a large number of observables. We have worked in the limit of heavy quark $m_b \to \infty$ and large energy $E_{K_2^*} \to \infty$, where symmetry relations reduce the number of independent form factors from seven to two: $\xi_\perp(q^2)$ and $\xi_\parallel(q^2)$. Utilizing these symmetry relations, we have provided expressions for transversity amplitudes, and have constructed new clean angular observables. The form-factor dependences for these clean observables cancel at leading order in α_s and $\Lambda_{\rm QCD}/m_b$. The uncertainties due to the subleading corrections have been included in our numerical analysis.

We have presented determinations of the $B \to K_2^*(\to K\pi)\mu^+\mu^-$ decay rate, forward-backward asymmetry, longitudinal polarization fractions, and clean observables in the SM and several NP cases. The NP scenarios are motivated by the recent global fits to the $b \to s\ell^+\ell^-$ data. We have also considered the LFU-violation-sensitive observable $R_{K_2^*}$. The $B \to K_2^*(\to K\pi)\mu^+\mu^-$ decay may provide new and complementary information to $B \to K^*(K)\mu^+\mu^-$ in searches of NP.

ACKNOWLEDGMENTS

D. D. is supported by the DST Government of India, under the INSPIRE Faculty Award (Grant No. DST/ 502 INSPIRE/04/2016/002620) India for financial support under the INSPIRE Faculty Fellowship. Authors would like to thank Gagan Mohanty and Saurabh Sandilya for useful discussions.

APPENDIX A: EFFECTIVE WILSON COEFFICIENTS FOR $b \to s\ell^+\ell^-$ TRANSITION

Corresponding to the $b \to s\ell^+\ell^-$ effective Hamiltonian in Eq. (1), the one-loop contributions from operators $\mathcal{O}_1$–$\mathcal{O}_6$ to $\mathcal{O}_7$ and $\mathcal{O}_9$ are absorbed by defining the effective Wilson coefficients $C_7^{\rm eff}$ and $C_9^{\rm eff}$ [41]:

TABLE III. Values of SM Wilson coefficients taken from Ref. [41].

	C_1	C_2	C_3	C_4	C_5	C_6	C_7	C_8	C_9	C_{10}
$\mu = 2.1$ GeV	−0.4965	1.0246	−0.0143	−0.1500	0.0010	0.0032	−0.3782	−0.2133	4.5692	−4.1602
$\mu = 4.2$ GeV	−0.2877	1.0101	−0.0060	−0.0860	0.0004	0.0011	−0.3361	−0.1821	4.2745	−4.1602
$\mu = 8.4$ GeV	−0.1488	1.0036	−0.0027	−0.0543	0.0002	0.0004	−0.3036	−0.1629	3.8698	−4.1602

$$
\begin{aligned}
C_7^{\rm eff}(\mu) &= C_7 - \frac{1}{3}C_3 + \frac{4}{3}C_4 + 20C_5 + \frac{80}{3}C_6 \\
&\quad - \frac{\alpha_S}{4\pi}[(C_1 - 6C_2)F_{1,c}^{(7)}(q^2) + C_8 F_8^{(7)}(q^2)], \\
C_9^{\rm eff}(\mu) &= C_9 + h(q^2, m_c)\left(\frac{4}{3}C_1 + C_2 + 6C_3 + 60C_5\right) \\
&\quad - \frac{1}{2}h(q^2, m_b)\left(7C_3 + \frac{4}{3}C_4 + 76C_5 + \frac{64}{3}C_6\right) \\
&\quad - \frac{1}{2}h(q^2, 0)\left(C_3 + \frac{4}{3}C_4 + 16C_5 + \frac{64}{3}C_6\right) \\
&\quad + \frac{4}{3}C_3 + \frac{64}{9}C_5 + \frac{64}{27}C_6 - \frac{\alpha_S}{4\pi}[C_1 F_{1,c}^{(9)}(q^2) \\
&\quad + C_2 F_{2,c}^{(9)}(q^2) + C_8 F_8^{(9)}(q^2)]. \qquad \text{(A1)}
\end{aligned}
$$

The value of the SM Wilson coefficients C_i $(i = 1, 2, \ldots 10)$ are given in Table III. The functions $h(q^2, m_q)$ and $F_8^{(7,9)}(q^2)$ can be found in Ref. [42], and the functions $F_{1,2}^{(7,9)}(q^2)$ are taken from Ref. [59]. The values of the masses of charm and bottom quarks in these expressions are defined in the pole mass scheme and are given in Table I.

APPENDIX B: K_2^* POLARIZATION TENSORS

The tensor meson K_2^* is described in terms of the spin-2 polarization tensor $\epsilon^{\mu\nu}(n)$, where the helicity n can be ± 2, ± 1, or 0. The polarization tensor satisfies $\epsilon^{\mu\nu}k^\nu = 0$. For the K_2^* which has four-momentum $(k_0, 0, 0, \vec{k})$, the polarization tensor $\epsilon^{\mu\nu}(h)$ can be constructed in terms of following polarization tensors [45],

$$
\epsilon_\mu(0) = \frac{1}{m_{K_2^*}}(|\vec{k}|, 0, 0, k_0), \qquad \epsilon_\mu(\pm) = \frac{1}{\sqrt{2}}(0, \mp 1, -i, 0),
$$

in the following way:

$$
\begin{aligned}
\epsilon_{\mu\nu}(\pm 2) &= \epsilon_\mu(\pm 1)\epsilon_\nu(\pm 1), \\
\epsilon_{\mu\nu}(\pm 1) &= \frac{1}{\sqrt{2}}[\epsilon_\nu(\pm)\epsilon_\nu(0) + \epsilon_\nu(\pm)\epsilon_\mu(0)], \\
\epsilon_{\mu\nu}(0) &= \frac{1}{\sqrt{6}}[\epsilon_\mu(+)\epsilon_\nu(-) + \epsilon_\nu(+)\epsilon_\mu(-)] + \sqrt{\frac{2}{3}}\epsilon_\mu(0)\epsilon_\nu(0).
\end{aligned}
$$

In the decay under consideration, since there are two leptons in the final state, the $n = \pm 2$ helicity states of the K_2^* are not realized. It is therefore convenient to introduce a new polarization vector [32]

$$
\epsilon_{T\mu}(h) = \frac{\epsilon_{\mu\nu}p^\nu}{m_B},
$$

where p is the four-momentum of the B meson. The explicit expressions of polarization vectors are

$$
\epsilon_{T\mu}(\pm 1) = \frac{1}{m_B}\frac{1}{\sqrt{2}}\epsilon(0).p\epsilon_\mu(\pm) = \frac{\sqrt{\lambda}}{\sqrt{8}m_B m_{K_2}^*}\epsilon_\mu(\pm), \qquad \text{(B1)}
$$

$$
\epsilon_{T\mu}(0) = \frac{1}{m_B}\sqrt{\frac{2}{3}}\epsilon(0).p\epsilon_\mu(0) = \frac{\sqrt{\lambda}}{\sqrt{6}m_B m_{K_2}^*}\epsilon_\mu(0), \qquad \text{(B2)}
$$

where $\lambda = m_B^4 + m_{K_2^*}^4 + q^4 - 2(m_B^2 m_{K_2^*}^2 + m_B^2 q^2 + m_{K_2^*}^2 q^2)$.

APPENDIX C: ANGULAR COEFFICIENTS $I_i(q^2)$

Here we summarize the expressions of the angular coefficients appearing in the differential decay rate [Eq. (20)] in terms of transversity amplitudes [38]

$$
\begin{aligned}
I_1^c &= (|A_{0L}|^2 + |A_{0R}|^2) + 8\frac{m_\ell^2}{q^2}\mathrm{Re}[A_{0L}A_{0R}^*] + 4\frac{m_\ell^2}{q^2}|A_t|^2, \\
I_1^s &= \frac{3}{4}\left(1 - \frac{4m_\ell^2}{3q^2}\right)[|A_{\perp L}|^2 + |A_{\parallel L}|^2 + |A_{\perp R}|^2 + |A_{\parallel R}|^2] \\
&\quad + \frac{4m_\ell^2}{q^2}\mathrm{Re}[A_{\perp L}A_{\perp R}^* + A_{\parallel L}A_{\parallel R}^*], \\
I_2^c &= -\beta_\ell^2(|A_{0L}|^2 + |A_{0R}|^2), \\
I_2^s &= \frac{1}{4}\beta_l^2(|A_{\perp L}|^2 + |A_{\parallel L}|^2 + |A_{\perp R}|^2 + |A_{\parallel R}|^2), \\
I_3 &= \frac{1}{2}\beta_l^2(|A_{\perp L}|^2 - |A_{\parallel L}|^2 + |A_{\perp R}|^2 - |A_{\parallel R}|^2), \\
I_4 &= \frac{1}{\sqrt{2}}\beta_\ell^2[\mathrm{Re}(A_{0L}A_{\parallel L}^*) + \mathrm{Re}(A_{0R}A_{\parallel R}^*], \\
I_5 &= \sqrt{2}\beta_l[\mathrm{Re}(A_{0L}A_{\perp L}^*) - \mathrm{Re}(A_{0R}A_{\perp R}^*)], \\
I_6 &= 2\beta_\ell[\mathrm{Re}(A_{\parallel L}A_{\perp L}^*) - \mathrm{Re}(A_{\parallel R}A_{\perp R}^*)], \\
I_7 &= \sqrt{2}\beta_\ell[\mathrm{Im}(A_{0L}A_{\parallel L}^*) - \mathrm{Im}(A_{0R}A_{\parallel R}^*)], \\
I_8 &= \frac{1}{\sqrt{2}}\beta_\ell^2[\mathrm{Im}(A_{0L}A_{\perp L}^*) + \mathrm{Im}(A_{0R}A_{\perp R}^*)], \\
I_9 &= \beta_\ell^2[\mathrm{Im}(A_{\parallel L}A_{\perp L}^*) + \mathrm{Im}(A_{\parallel R}A_{\perp R}^*)], \qquad \text{(C1)}
\end{aligned}
$$

where $\beta_\ell = \sqrt{1 - \frac{4m_\ell^2}{q^2}}$.

APPENDIX D

1. Prediction of observables in the SM

Bin	P_1	P_2	P_3
[0.1, 1]	-0.001 ± 0.058	0.125 ± 0.004	0.0 ± 0.029
[1, 2]	-0.001 ± 0.058	0.431 ± 0.010	0.0 ± 0.029
[2, 4]	-0.001 ± 0.058	0.186 ± 0.041	0.0 ± 0.029
[4, 6]	-0.001 ± 0.058	-0.284 ± 0.028	0.0 ± 0.029
[1, 6]	-0.001 ± 0.058	0.001 ± 0.035	0.0 ± 0.029

Bin	P_4'	P_5'	P_6'
[0.1, 1]	-0.530 ± 0.016	0.615 ± 0.020	0.036 ± 0.039
[1, 2]	-0.178 ± 0.021	$0.235 \pm 0.0.031$	0.044 ± 0.021
[2, 4]	0.533 ± 0.037	-0.493 ± 0.048	0.039 ± 0.033
[4, 6]	0.886 ± 0.028	-0.869 ± 0.033	0.023 ± 0.053
[1, 6]	0.551 ± 0.033	-0.519 ± 0.041	0.033 ± 0.034

Bin	$\mathrm{BR}(10^{-7})$	A_{FB}	F_L
[0.1, 1]	0.204 ± 0.093	0.092 ± 0.028	0.350 ± 0.199
[1, 2]	0.104 ± 0.056	0.193 ± 0.127	0.691 ± 0.205
[2, 4]	0.197 ± 0.113	0.066 ± 0.056	0.764 ± 0.188
[4, 6]	0.233 ± 0.124	-0.135 ± 0.089	0.684 ± 0.207
[1, 6]	0.534 ± 0.292	0.001 ± 0.018	0.714 ± 0.201

2. Prediction of observables in the NP scenario S1 ($C_9^{\mu,\mathrm{NP}} = -1.02$)

Bin	P_1	P_2	P_3
[0.1, 1]	-0.001 ± 0.058	0.123 ± 0.004	0.0 ± 0.029
[1, 2]	-0.001 ± 0.058	0.409 ± 0.011	0.0 ± 0.029
[2, 4]	-0.001 ± 0.058	0.355 ± 0.026	0.0 ± 0.029
[4, 6]	-0.001 ± 0.058	-0.069 ± 0.036	0.0 ± 0.029
[1, 6]	-0.001 ± 0.058	0.181 ± 0.029	0.0 ± 0.029

Bin	P_4'	P_5'	P_6'
[0.1, 1]	-0.421 ± 0.012	0.731 ± 0.023	0.039 ± 0.046
[1, 2]	-0.101 ± 0.014	0.434 ± 0.028	0.045 ± 0.031
[2, 4]	0.478 ± 0.031	-0.165 ± 0.048	0.041 ± 0.018
[4, 6]	0.843 ± 0.028	-0.628 ± 0.041	0.027 ± 0.039
[1, 6]	0.509 ± 0.029	-0.236 ± 0.045	0.036 ± 0.020

Bin	$\mathrm{BR}(10^{-7})$	A_{FB}	F_L
[0.1, 1]	0.197 ± 0.092	0.099 ± 0.026	0.298 ± 0.186
[1, 2]	0.094 ± 0.046	0.230 ± 0.127	0.610 ± 0.216
[2, 4]	0.167 ± 0.091	0.156 ± 0.109	0.706 ± 0.202
[4, 6]	0.191 ± 0.099	-0.035 ± 0.031	0.657 ± 0.211
[1, 6]	0.452 ± 0.235	0.091 ± 0.059	0.665 ± 0.210

3. Prediction of observables in the NP scenario S2 ($C_9^{\mu,\mathrm{NP}} = -C_{10}^{\mu,\mathrm{NP}} = -0.49$)

Bin	P_1	P_2	P_3
[0.1, 1]	-0.001 ± 0.058	0.110 ± 0.004	0.0 ± 0.029
[1, 2]	-0.001 ± 0.058	0.394 ± 0.011	0.0 ± 0.029
[2, 4]	-0.001 ± 0.058	0.300 ± 0.035	0.0 ± 0.029
[4, 6]	-0.001 ± 0.058	-0.210 ± 0.036	0.0 ± 0.029
[1, 6]	-0.001 ± 0.058	0.096 ± 0.035	0.0 ± 0.029

Bin	P_4'	P_5'	P_6'
[0.1, 1]	-0.544 ± 0.016	0.635 ± 0.020	0.035 ± 0.040
[1, 2]	-0.258 ± 0.017	0.321 ± 0.028	0.043 ± 0.025
[2, 4]	0.410 ± 0.039	-0.359 ± 0.052	0.042 ± 0.027
[4, 6]	0.845 ± 0.030	-0.821 ± 0.037	0.027 ± 0.050
[1, 6]	0.449 ± 0.035	-0.408 ± 0.046	0.036 ± 0.028

Bin	$\mathrm{BR}(10^{-7})$	A_{FB}	F_L
[0.1, 1]	0.191 ± 0.090	0.087 ± 0.023	0.299 ± 0.187
[1, 2]	0.088 ± 0.044	0.206 ± 0.121	0.637 ± 0.213
[2, 4]	0.155 ± 0.088	0.112 ± 0.088	0.749 ± 0.192
[4, 6]	0.179 ± 0.096	-0.098 ± 0.068	0.690 ± 0.206
[1, 6]	0.422 ± 0.227	0.043 ± 0.035	0.699 ± 0.204

4. Prediction of observables in the NP scenario S3 ($C_9^{\mu,\mathrm{NP}} = -C_9^{\prime\mu,\mathrm{NP}} = -1.02$)

Bin	P_1	P_2	P_3
[0.1, 1]	0.056 ± 0.058	0.123 ± 0.004	0.001 ± 0.029
[1, 2]	0.194 ± 0.056	0.404 ± 0.011	0.005 ± 0.028
[2, 4]	0.164 ± 0.058	0.339 ± 0.025	0.007 ± 0.026
[4, 6]	-0.033 ± 0.060	-0.065 ± 0.034	0.004 ± 0.026
[1, 6]	0.083 ± 0.059	0.174 ± 0.028	0.005 ± 0.026

Bin	P_4'	P_5'	P_6'
[0.1, 1]	-0.247 ± 0.008	0.876 ± 0.026	0.043 ± 0.052
[1, 2]	0.127 ± 0.016	0.694 ± 0.026	0.049 ± 0.034
[2, 4]	0.699 ± 0.035	0.207 ± 0.047	0.045 ± 0.020
[4, 6]	0.997 ± 0.030	-0.251 ± 0.045	0.030 ± 0.042
[1, 6]	0.704 ± 0.032	0.110 ± 0.046	0.039 ± 0.021

Bin	$\mathrm{BR}(10^{-7})$	A_{FB}	F_L
[0.1, 1]	0.187 ± 0.090	0.103 ± 0.025	0.262 ± 0.174
[1, 2]	0.083 ± 0.039	0.252 ± 0.127	0.566 ± 0.218
[2, 4]	0.145 ± 0.075	0.172 ± 0.108	0.661 ± 0.210
[4, 6]	0.168 ± 0.083	-0.038 ± 0.031	0.607 ± 0.217
[1, 6]	0.396 ± 0.196	0.099 ± 0.059	0.617 ± 0.215

5. Prediction of $R_{K_2^*}$

Bin	SM	S1	S2	S3
[0.1, 1]	0.984 ± 0.005	0.945 ± 0.056	0.920 ± 0.051	0.963 ± 0.050
[1, 2]	0.997 ± 0.003	0.922 ± 0.092	0.855 ± 0.057	0.954 ± 0.090
[2, 4]	0.996 ± 0.002	0.868 ± 0.067	0.790 ± 0.015	0.898 ± 0.065
[4, 6]	0.996 ± 0.002	0.823 ± 0.026	0.762 ± 0.007	0.845 ± 0.024
[1, 6]	0.996 ± 0.002	0.859 ± 0.052	0.790 ± 0.014	0.885 ± 0.050

[1] R. Aaij *et al.* (LHCb Collaboration), Test of lepton universality using $B^+ \to K^+\ell^+\ell^-$ decays, Phys. Rev. Lett. **113**, 151601 (2014).

[2] R. Aaij *et al.* (LHCb Collaboration), Test of lepton universality with $B^0 \to K^{*0}\ell^+\ell^-$ decays, J. High Energy Phys. 08 (2017) 055.

[3] S. Descotes-Genon, J. Matias, and J. Virto, Understanding the $B \to K^*\mu^+\mu^-$ anomaly, Phys. Rev. D **88**, 074002 (2013).

[4] R. Aaij *et al.* (LHCb Collaboration), Measurement of Form-Factor-Independent Observables in the Decay $B^0 \to K^{*0}\mu^+\mu^-$, Phys. Rev. Lett. **111**, 191801 (2013).

[5] R. Aaij *et al.* (LHCb Collaboration), Angular analysis of the $B^0 \to K^{*0}\mu^+\mu^-$ decay using 3 fb^{-1} of integrated luminosity, J. High Energy Phys. 02 (2016) 104.

[6] A. Abdesselam *et al.* (Belle Collaboration), Angular analysis of $B^0 \to K^*(892)^0\ell^+\ell^-$, in *Proceedings, LHCSki 2016: A First Discussion of 13 TeV Results, Obergurgl, Austria, 2016* (2016) [arXiv:1604.04042].

[7] S. Wehle *et al.* (Belle Collaboration), Lepton-flavor-dependent angular analysis of $B \to K^*\ell^+\ell^-$, Phys. Rev. Lett. **118**, 111801 (2017).

[8] T. Aaltonen *et al.* (ATLAS Collaboration), Angular analysis of $B_d^0 \to K^*\mu^+\mu^-$ decays in pp collisions at $\sqrt{s} = 8$ TeV with the ATLAS detector, J. High Energy Phys. 10 (2018) 047.

[9] CMS Collaboration, Measurement of the P_1 and P_5' angular parameters of the decay $\mathrm{B}^0 \to \mathrm{K}^{*0}\mu^+\mu^-$ in proton-proton collisions at $\sqrt{s} = 8$ TeV, Phys. Lett. B **781**, 517 (2018).

[10] R. Aaij *et al.* (LHCb Collaboration), Angular analysis and differential branching fraction of the decay $B_s^0 \to \phi\mu^+\mu^-$, J. High Energy Phys. 09 (2015) 179.

[11] S. Descotes-Genon, L. Hofer, J. Matias, and J. Virto, Global analysis of $b \to s\ell\ell$ anomalies, J. High Energy Phys. 06 (2016) 092.

[12] W. Altmannshofer and D. M. Straub, New physics in $b \to s$ transitions after LHC run 1, Eur. Phys. J. C **75**, 382 (2015).

[13] T. Hurth, F. Mahmoudi, and S. Neshatpour, On the anomalies in the latest LHCb data, Nucl. Phys. **B909**, 737 (2016).

[14] W. Altmannshofer and D. M. Straub, Implications of $b \to s$ measurements, in *Proceedings, 50th Rencontres de Moriond Electroweak Interactions and Unified Theories, La Thuile, Italy, 2015* (2015), pp. 333–338 [arXiv:1503.06199].

[15] W. Altmannshofer and D. M. Straub, New physics in $B \to K^*\mu\mu$?, Eur. Phys. J. C **73**, 2646 (2013).

[16] F. Beaujean, C. Bobeth, and D. van Dyk, Comprehensive Bayesian analysis of rare (semi)leptonic and radiative B decays, Eur. Phys. J. C **74**, 2897 (2014); Erratum, Eur. Phys. J. C**74**, 3179(E) (2014).

[17] T. Hurth and F. Mahmoudi, On the LHCb anomaly in $B \to K^*\ell^+\ell^-$, J. High Energy Phys. 04 (2014) 097.

[18] B. Capdevila, A. Crivellin, S. Descotes-Genon, J. Matias, and J. Virto, Patterns of new physics in $b \to s\ell^+\ell^-$ transitions in the light of recent data, J. High Energy Phys. 01 (2018) 093.

[19] A. K. Alok, A. Dighe, S. Gangal, and D. Kumar, Continuing search for new physics in $b \to s\mu\mu$ decays: Two operators at a time, arXiv:1903.09617.

[20] M. Ciuchini, A. M. Coutinho, M. Fedele, E. Franco, A. Paul, L. Silvestrini, and M. Valli, New physics in $b \to s\ell^+\ell^-$ confronts new data on lepton universality, arXiv:1903.09632.

[21] G. D'Amico, M. Nardecchia, P. Panci, F. Sannino, A. Strumia, R. Torre, and A. Urbano, Flavour anomalies after the R_{K^*} measurement, J. High Energy Phys. 09 (2017) 010.

[22] A. Datta, J. Kumar, and D. London, The B anomalies and new physics in $b \to se^+e^-$, arXiv:1903.10086.

[23] J. Aebischer, W. Altmannshofer, D. Guadagnoli, M. Reboud, P. Stangl, and D. M. Straub, B-decay discrepancies after Moriond 2019, arXiv:1903.10434.

[24] M. Algueró, B. Capdevila, A. Crivellin, S. Descotes-Genon, P. Masjuan, J. Matias, and J. Virto, Addendum: "Patterns of new physics in $b \to s\ell^+\ell^-$ transitions in the light of recent data" and "Are we overlooking lepton flavour universal new physics in $b \to s\ell\ell$?", arXiv:1903.09578.

[25] B. Aubert *et al.* (*BABAR* Collaboration), Measurement of the $B^0 \to K_2^*(1430)^0\gamma$ and $B^+ \to K_2^*(1430)^+\gamma$ branching fractions, Phys. Rev. D **70**, 091105 (2004).

[26] S. Nishida *et al.* (Belle Collaboration), Radiative B Meson Decays into $K\pi\gamma$ and $K\pi\pi\gamma$ Final States, Phys. Rev. Lett. **89**, 231801 (2002).

[27] R. Aaij *et al.* (LHCb Collaboration), Differential branching fraction and angular moments analysis of the decay $B^0 \to K^+\pi^-\mu^+\mu^-$ in the $K_{0,2}^*(1430)^0$ region, J. High Energy Phys. 12 (2016) 065.

[28] S. R. Choudhury, A. S. Cornell, G. C. Joshi, and B. H. J. McKellar, Analysis of the $B \to K_2^*(\to K\pi)l + l-$ decay, Phys. Rev. D **74**, 054031 (2006).

[29] S. R. Choudhury, A. S. Cornell, and N. Gaur, Analysis of the $\bar{B} \to \bar{K}_2(1430)l + l-$ decay, Phys. Rev. D **81**, 094018 (2010).

[30] H. Hatanaka and K.-C. Yang, Radiative and semileptonic B decays involving the tensor meson $K_2^*(1430)$ in the standard model and beyond, Phys. Rev. D **79**, 114008 (2009).

[31] H. Hatanaka and K.-C. Yang, Radiative and semileptonic B decays involving higher K-resonances in the final states, Eur. Phys. J. C **67**, 149 (2010).

[32] W. Wang, B to tensor meson form factors in the perturbative QCD approach, Phys. Rev. D **83**, 014008 (2011).

[33] H.-Y. Cheng, Y. Koike, and K.-C. Yang, Two-parton light-cone distribution amplitudes of tensor mesons, Phys. Rev. D **82**, 054019 (2010).

[34] Z.-G. Wang, Analysis of the $B \to K_2^*(1430)$, $a_2(1320)$, $f_2(1270)$ form-factors with light-cone QCD sum rules, Mod. Phys. Lett. A **26**, 2761 (2011).

[35] K.-C. Yang, B to light tensor meson form factors derived from light-cone sum rules, Phys. Lett. B **695**, 444 (2011).

[36] I. Ahmed, M. J. Aslam, M. Junaid, and S. Shafaq, Model independent analysis of $B \to K_2^*(1430)\mu^+\mu^-$ decay, J. High Energy Phys. 02 (2012) 045.

[37] M. Junaid, M. J. Aslam, and I. Ahmed, Complementarity of semileptonic B to $K_2^*(1430)$ and $K^*(892)$ decays in the Standard Model with fourth generation, Int. J. Mod. Phys. A **27**, 1250149 (2012).

[38] R.-H. Li, C.-D. Lu, and W. Wang, Branching ratios, forward-backward asymmetries and angular distributions of $B \to K_2^* l^+ l^-$ in the Standard Model and new physics scenarios, Phys. Rev. D **83**, 034034 (2011).

[39] C.-D. Lu and W. Wang, Analysis of $B \to K_J^*(\to K\pi)\mu^+\mu^-$ in the higher kaon resonance region, Phys. Rev. D **85**, 034014 (2012).

[40] T. M. Aliev and M. Savci, $B \to K_2 \ell^+ \ell^-$ decay beyond the Standard Model, Phys. Rev. D **85**, 015007 (2012).
[41] W. Detmold and S. Meinel, $\Lambda_b \to \Lambda \ell^+ \ell^-$ form factors, differential branching fraction, and angular observables from lattice QCD with relativistic b quarks, Phys. Rev. D **93**, 074501 (2016).
[42] M. Beneke, T. Feldmann, and D. Seidel, Systematic approach to exclusive $B \to V l^+ l^-$, $V\gamma$ decays, Nucl. Phys. **B612**, 25 (2001).
[43] M. Beneke, T. Feldmann, and D. Seidel, Exclusive radiative and electroweak $b \to d$ and $b \to s$ penguin decays at NLO, Eur. Phys. J. C **41**, 173 (2005).
[44] A. Paul and D. M. Straub, Constraints on new physics from radiative B decays, J. High Energy Phys. 04 (2017) 027.
[45] E. R. Berger, A. Donnachie, H. G. Dosch, and O. Nachtmann, Observing the odderon: Tensor meson photoproduction, Eur. Phys. J. C **14**, 673 (2000).
[46] M. J. Dugan and B. Grinstein, QCD basis for factorization in decays of heavy mesons, Phys. Lett. B **255**, 583 (1991).
[47] J. Charles, A. Le Yaouanc, L. Oliver, O. Pene, and J. C. Raynal, Heavy to light form-factors in the heavy mass to large energy limit of QCD, Phys. Rev. D **60**, 014001 (1999).
[48] M. Wirbel, B. Stech, and M. Bauer, Exclusive semileptonic decays of heavy mesons, Z. Phys. C **29**, 637 (1985).
[49] U. Egede, T. Hurth, J. Matias, M. Ramon, and W. Reece, New physics reach of the decay mode $\bar{B} \to \bar{K}^{*0} \ell^+ \ell^-$, J. High Energy Phys. 10 (2010) 056.
[50] W. Altmannshofer, P. Ball, A. Bharucha, A. J. Buras, D. M. Straub, and M. Wick, Symmetries and asymmetries of $B \to K^* \mu^+ \mu^-$ decays in the Standard Model and beyond, J. High Energy Phys. 01 (2009) 019.
[51] J. Gratrex, M. Hopfer, and R. Zwicky, Generalised helicity formalism, higher moments and the $B \to K_{J_K} (\to K\pi) \bar{\ell}_1 \ell_2$ angular distributions, Phys. Rev. D **93**, 054008 (2016).
[52] M. Tanabashi *et al.* (Particle Data Group), Review of particle physics, Phys. Rev. D **98**, 030001 (2018).
[53] UTfit, http://www.utfit.org/UTfit/ResultsSummer2014PostMoriondSM.
[54] S. Descotes-Genon, T. Hurth, J. Matias, and J. Virto, Optimizing the basis of $B \to K^* ll$ observables in the full kinematic range, J. High Energy Phys. 05 (2013) 137.
[55] J. Matias, F. Mescia, M. Ramon, and J. Virto, Complete anatomy of $\bar{B}_d - > \bar{K}^{*0} (\to K\pi) l^+ l^-$ and its angular distribution, J. High Energy Phys. 04 (2012) 104.
[56] S. Descotes-Genon, J. Matias, M. Ramon, and J. Virto, Implications from clean observables for the binned analysis of $B - > K * \mu^+ \mu^-$ at large recoil, J. High Energy Phys. 01 (2013) 048.
[57] M. Bordone, G. Isidori, and A. Pattori, On the Standard Model predictions for R_K and R_{K^*}, Eur. Phys. J. C **76**, 440 (2016).
[58] G. Hiller and I. Nisandzic, R_K and R_{K^*} beyond the Standard Model, Phys. Rev. D **96**, 035003 (2017).
[59] H. H. Asatryan, H. M. Asatrian, C. Greub, and M. Walker, Calculation of two loop virtual corrections to $b \to s l^+ l^-$ in the Standard Model, Phys. Rev. D **65**, 074004 (2002).